

PAPER

Pilot-Assisted Channel Estimation Using Adaptive Interpolation for Coherent Rake Reception of DS-CDMA Signals

Shinsuke TAKAOKA^{†a)}, *Student Member and Fumiyuki ADACHI[†], Member*

SUMMARY In this paper, a pilot-assisted channel estimation using adaptive interpolation (in which, different interpolation filter tap weights is used for different symbol position) is proposed. Each set of tap weights is updated using the normalized least mean square (NLMS) algorithm, the reference signal for which is obtained by decision feedback and reverse modulation of the received data symbol. In order to reduce the number of tap weight sets and to achieve fast convergence, the conjugate centrosymmetry property of the tap weight set is used. The average bit error rate (BER) performance in a frequency-selective Rayleigh fading channel is evaluated by computer simulation. Also evaluated is the robustness against the frequency offset between a transmitter and a receiver.

key words: DS-CDMA, adaptive interpolation, conjugate centrosymmetry property, fast convergence

1. Introduction

Direct sequence code division multiple access (DS-CDMA) is used in present cellular mobile communications systems [1]. In mobile radio, the transmitted signal is reflected and diffracted by many obstacles between a transmitter and a receiver, thus creating the multipath fading channel [2]. For coherent rake reception of DS-CDMA signals, accurate channel estimation is necessary and so far many channel estimation schemes have been studied [3]–[7]. Pilot-assisted channel estimation called weighted multi-slot averaging (WMSA) channel estimation using a finite impulse response (FIR) filter with time-invariant fixed tap weights was proposed for coherent rake reception of DS-CDMA signals [6]. However, using the time-invariant fixed tap weights cannot always minimize the bit error rate (BER) performance in a changing multipath propagation environment due to user's movement. Hence, adaptive channel estimation schemes were proposed in [8]–[10].

In addition to fading, the presence of the frequency offset between a transmitter and a receiver may degrade the BER performance due to constant phase rotation in the received signal. Thus, adaptive prediction channel estimation proposed in [10] uses the complex-valued tap weights to track the constant phase rotation due to the frequency offset in addition to random phase rotation due to fading. In this scheme, the instantaneous channel gain at each data symbol position in a slot is estimated by simple averaging (SA)

or linear interpolation (LI) using the two predicted instantaneous channel gains obtained from adaptive backward and forward predictors. However, as fading becomes faster, the tracking capability against fading tends to be lost due to the use of SA or LI [10].

For achieving good tracking capability against fading and frequency offset, a pilot-assisted channel estimation using Wiener filter [3] is desirable. However, Wiener filter requires the knowledge of the channel statistics, e.g., the maximum Doppler frequency, the frequency offset and the average received signal-to-noise power ratio (SNR), which are in general unknown to a receiver. Thus, in order to achieve better channel estimation in various channel conditions, some adaptive techniques must be adopted.

In this paper, a pilot-assisted channel estimation using adaptive interpolation is proposed to estimate the channel gains at different symbol positions in a slot for the coherent rake reception of DS-CDMA signals. The proposed scheme jointly estimates the fading channel gain and the constant phase rotation due to the frequency offset. Each set of interpolation filter tap weights is updated using the normalized least mean square (NLMS) algorithm based on the minimum mean square error (MMSE) criterion. Hence, a high adaptability to changing channel condition is achieved compared to [10]. Furthermore, the proposed channel estimation scheme has a better tracking capability against fast fading and frequency offset, compared to the channel estimation of [10], [14]. In order to reduce the number of tap weight sets and to achieve fast convergence, the conjugate centrosymmetry property [11], [12] of tap weight set is used.

The remainder of this paper is organized as follows. In Sect. 2, an overall transmission system model and the operation principle of the proposed adaptive channel estimation are described. Section 3 presents the computer simulation results in a frequency-selective Rayleigh fading channel and compares the simulation results with those using the non-adaptive WMSA channel estimation [6] and the adaptive prediction channel estimation [10]. Also discussed is the BER performance in the presence of frequency offset between a transmitter and a receiver. Section 4 concludes the paper.

2. Adaptive Channel Estimation

2.1 Received Signal Representation

The transmission system model and the slot structure are

Manuscript received August 26, 2004.

Manuscript revised January 19, 2005.

[†]The authors are with the Department of Electrical and Communication Engineering, Graduate School of Engineering, Tohoku University, Sendai-shi, 980-8579 Japan.

a) E-mail: takaoka@mobile.ecei.tohoku.ac.jp

DOI: 10.1093/ietcom/e88-b.7.2962

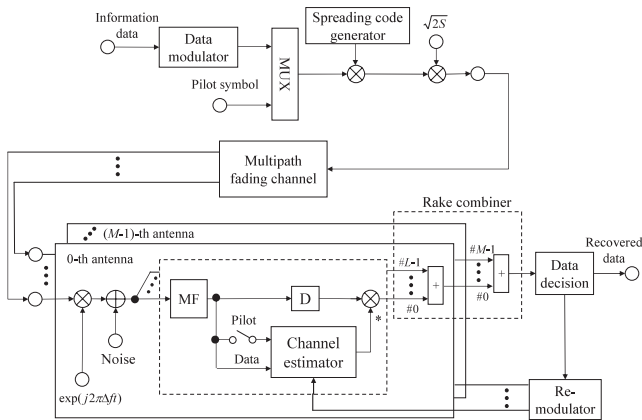


Fig. 1 Transmission system model.

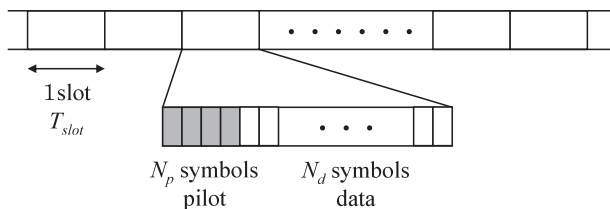


Fig. 2 Slot structure.

illustrated in Figs. 1 and 2, respectively. At the transmitter, a binary data to be transmitted is transformed into data-modulated symbol sequence. Then, a block of known N_p pilot symbols is time-multiplexed every N_d data symbols as shown in Fig. 2. N_p pilot symbols and succeeding N_d data symbols constitute a data slot with a length of $T_{slot} = (N_p + N_d)T$, where T denotes symbol length. Finally, the pilot-inserted symbol sequence is multiplied by a spreading sequence to produce the DS-CDMA signal $s(t)$, which is transmitted over a multipath propagation channel. It is assumed that the propagation channel is frequency-selective and has L discrete paths having T_c -spaced time delays and experiencing independent fading, where T_c is the chip duration. The complex path gain and time delay of the l th path are represented as $\xi_{m,l}(t)$ and τ_l , respectively, with $E[\sum_{l=0}^{L-1} |\xi_{m,l}(t)|^2] = 1$; $E[\cdot]$ is the ensemble average operation. The receiver has a total of M spatially separated antennas ($m = 0 \sim M - 1$).

The received signal $r_m(t)$ on the m th antenna can be expressed, using the lowpass equivalent representation, as

$$r_m(t) = \sum_{l=0}^{L-1} \xi_{m,l}(t) \exp(j2\pi\Delta f t) s(t - \tau_l) + v_m(t), \quad (1)$$

where Δf is the frequency offset between the transmitter and the receiver, $s(t)$ is the transmitted DS-CDMA signal, and $v_m(t)$ represents the additive white Gaussian noise (AWGN) having the single-sided power spectrum density of N_0 . We have assumed that the receiver filter is wide enough not to distort the received signal at all due to the frequency offset. The received faded/phase-rotated DS-CDMA signal $r_m(t)$ is

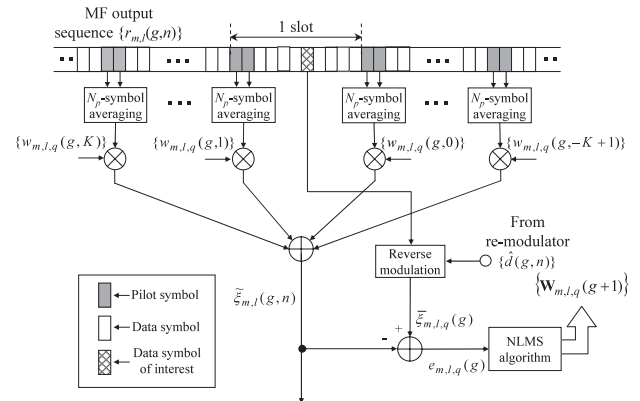


Fig. 3 Block diagram of adaptive channel estimator.

despread and resolved into L copies of transmitted symbol sequence by a bank of matched filters (MFs). The MF output $r_{m,l}(g,n)$ at the n th symbol time epoch of the g th slot, associated with the l th path, is represented as

$$\begin{aligned} r_{m,l}(g,n) &= \frac{1}{T} \int_{gT_{slot}+nT+\tau_l}^{gT_{slot}+(n+1)T+\tau_l} r_m(t) p^*(t - \tau_l) dt \\ &= \sqrt{2S} \xi_{m,l}(g,n) d(g,n) \\ &\quad \times \exp[j2\pi\Delta f(gT_{slot} + nT)] + v_{m,l}(g,n), \end{aligned} \quad (2)$$

where $\xi_{m,l}(g,n) = \xi_{m,l}(gT_{slot} + nT)$, S and $p(t)$ represent the received signal power and the spreading sequence waveform, respectively, $d(g,n)$ and $v_{m,l}(g,n)$ represent the data symbol and the noise plus interpath interference (IPI) component, respectively, and $*$ denotes the complex conjugate operation. In the rake combiner, a total of $M \times L$ MF outputs are coherently summed up based on maximal ratio combining (MRC) [2]. The rake combiner output $\eta(g,n)$, which is the decision variable, can be expressed as

$$\eta(g,n) = \sum_{m=0}^{M-1} \sum_{l=0}^{L-1} r_{m,l}(g,n) \tilde{\xi}_{m,l}^*(g,n), \quad (3)$$

where $\tilde{\xi}_{m,l}(g,n)$ is the estimate of $\xi_{m,l}(g,n)$. Adaptive channel estimation proposed in this paper will be described in the following subsection.

2.2 Operation Principle of Proposed Channel Estimation Scheme

Figure 3 illustrates the block diagram of proposed adaptive channel estimator.

First, the instantaneous channel gain is estimated by coherent addition of N_p received pilot symbols as in the conventional WMSA channel estimation [6]. Without loss of generality, the pilot symbol $d = 1 + j0$ is assumed. The instantaneous channel estimate, $\hat{\xi}_{m,l}(g)$, at the beginning of the g th slot is given by

$$\hat{\xi}_{m,l}(g) = \frac{1}{N_p} \sum_{n=0}^{N_p-1} r_{m,l}(g,n). \quad (4)$$

Then, using the K past and K future instantaneous channel gains, $\{\hat{\xi}_{m,l}(g+k); k = -K+1 \sim K\}$, the channel gains at N_d different data symbol positions in the g th slot of interest are estimated by the $2K$ -tap adaptive interpolation filter. The channel gain estimate at the n th data symbol position of the g th slot, associated with the l th path, is given by

$$\begin{aligned}\tilde{\xi}_{m,l}(g, n) &= \sum_{k=-K+1}^K w_{m,l,q}(g, k) \hat{\xi}_{m,l}(g+k) \\ &= \mathbf{W}_{m,l,q}^T(g) \mathbf{X}_{m,l}(g)\end{aligned}\quad (5)$$

where $q = \lfloor \frac{n-N_p}{N_d/Q} \rfloor$ for $n = N_p \sim N_p + N_d - 1$, with

$$\begin{cases} \mathbf{W}_{m,l,q}(g) = [w_{m,l,q}(g, K), \dots, w_{m,l,q}(g, -K+1)]^T \\ \mathbf{X}_{m,l}(g) = [\hat{\xi}_{m,l}(g+K), \dots, \hat{\xi}_{m,l}(g-K+1)]^T \end{cases}, \quad (6)$$

where $\mathbf{W}_{m,l,q}(g)$ and $\mathbf{X}_{m,l}(g)$ are the adaptively updated $2K$ -by-1 complex tap weight vector of the q th weight set ($q = 0 \sim N_d - 1$) and the $2K$ -by-1 instantaneous channel gain estimate vector used for the g th slot, respectively, and $[\cdot]^T$ denotes transposition. The optimum $\mathbf{W}_{m,l,q}(g)$ is given by Eq. (A.1) of Appendix, and is determined by the fading statistical property, the average SNR and frequency offset. Since the frequency offset and the fading produce the constant phase rotation and the random phase rotation in the received signal, respectively, the optimum tap weights are in general complex. Thus, we use the complex tap weight vector in this paper (in the special case of Jakes fading model, the fading time auto-correlation is given by $J_0(2\pi f_D \tau)$ [2], where $J_0(2\pi f_D \tau)$ is the zero-th order Bessel function of first kind and f_D is the maximum Doppler frequency, and therefore the optimum tap weight vector becomes a real-valued one if the frequency offset is not present).

2.3 Reduction in Number of Tap Weight Sets

The adaptive channel estimator described in Sect. 2.2 requires the total number $2K \times N_d \times L \times M$ of tap weights. Reducing the number of available weight sets reduces the receiver complexity. In what follows, the reduction in the number of tap weight sets is presented.

Since the channel gain stays almost constant over several symbol durations if fading is not too fast, we can reduce the number of tap weight sets; Q tap weight sets $\{\mathbf{W}_{m,l,q}(g); q = 0 \sim Q-1\}$ are used instead of N_d tap weight sets, where $Q \leq N_d$ (with N_d/Q being an integer). The total number of tap weights is reduced to $2K \times Q \times L \times M$. Each tap weight set is shared for channel estimation at consecutive N_d/Q data symbol positions in a slot (i.e., $n = N_p + q(N_d/Q) \sim N_p + (q+1)(N_d/Q) - 1$). When $Q = N_d$, channel estimation is carried out at every data symbol position in a slot. On the other hand, when $Q=1$, channel estimation is carried out once in a slot and the same channel estimate is used for all data symbol positions. Reducing the number of available weight sets reduces the receiver complexity; however, the

achievable BER performance may degrade in a fast fading environment. The minimum number Q of available weight sets without BER degradation is discussed in Sect. 3.5.

In order to further reduce the number of tap weight sets, the conjugate centrosymmetry property [11], [12] of the tap weight sets is applied. From Appendix, Q sets of optimum tap weights have the following conjugate centrosymmetry property:

$$\mathbf{W}_{m,l,(Q-1)-q} = \mathbf{U} \mathbf{W}_{m,l,q}^* \quad \text{for } q = 0 \sim Q-1. \quad (7)$$

Equation (7) implies that the q th tap weight set $\mathbf{W}_{m,l,q}(g)$ for channel estimation at the data symbol positions of $n = N_p + q(N_d/Q) \sim N_p + (q+1)(N_d/Q) - 1$ can be reused for the channel estimation at the data symbol positions of $n = N_p + (Q-1-q)(N_d/Q) \sim N_p + ((Q-1-q)+1)(N_d/Q) - 1$, instead of using $((Q-1)-q)$ th tap weight set $\mathbf{W}_{m,l,(Q-1)-q}(g)$ (the matrix of \mathbf{U} reverses the element-order of a $2K$ -by-1 vector). Hence, this property allows to reduce the number of tap weight sets by half; the tap weight sets $\{\mathbf{W}_{m,l,q}(g); q = 0 \sim Q/2 - 1\}$ are used (note that the reduction in the number of tap weight sets using the conjugate centrosymmetry property does not cause any degradation in BER). Using Eq. (7), Eq. (5) can be rewritten as

$$\tilde{\xi}_{m,l}(g, n) = \mathbf{W}_{m,l,q}^T(g) \mathbf{X}_{m,l}(g) \quad (8a)$$

where $q = \lfloor \frac{n-N_p}{N_d/Q} \rfloor$ for $n = N_p \sim N_p + N_d/2 - 1$, and

$$\tilde{\xi}_{m,l}(g, n) = (\mathbf{U} \mathbf{W}_{m,l,q}^*(g))^T \mathbf{X}_{m,l}(g) \quad (8b)$$

where $q = Q-1 - \lfloor \frac{n-N_p}{N_d/Q} \rfloor$ for $n = N_p + N_d/2 \sim N_p + N_d - 1$. As a consequence, by using the conjugate centrosymmetry property, the total number of tap weights is reduced to $K \times Q \times L \times M$.

Assuming that the time auto-correlation of fading channel is the same for all antennas ($m = 0 \sim M-1$), the tap weight sets $\{\mathbf{W}_{m,l,q}(g); m = 0 \sim M-1\}$ can be reduced to one which is used for all antennas. By introducing the common tap weight sets $\{\mathbf{W}_{l,q}^{(\text{com})}(g); q = 0 \sim Q/2 - 1\}$ for all antennas in addition to using the conjugate centrosymmetry property, the number of the tap weight sets can be further reduced. Eqs. (8a) and (8b) can be rewritten as

$$\tilde{\xi}_{m,l}(g, n) = \mathbf{W}_{l,q}^{(\text{com})T}(g) \mathbf{X}_{m,l}(g) \quad (9a)$$

where $q = \lfloor \frac{n-N_p}{N_d/Q} \rfloor$ for $n = N_p \sim N_p + N_d/2 - 1$, and

$$\tilde{\xi}_{m,l}(g, n) = (\mathbf{U} \mathbf{W}_{l,q}^{(\text{com})*}(g))^T \mathbf{X}_{m,l}(g) \quad (9b)$$

where $q = Q-1 - \lfloor \frac{n-N_p}{N_d/Q} \rfloor$ for $n = N_p + N_d/2 \sim N_p + N_d - 1$. In Eqs. (9a) and (9b), $\mathbf{W}_{l,q}^{(\text{com})}(g) = [w_{l,q}^{(\text{com})}(g, K), \dots, w_{l,q}^{(\text{com})}(g, -K+1)]^T$ is the $2K$ -by-1 complex tap weight vector of the q th weight set ($q = 0 \sim Q/2 - 1$). When the common tap weight sets are used, the total number of tap weights is further reduced to $K \times Q \times L$.

2.4 Tap Weight Adaptation

For the adaptation of $2K$ tap weights, the simple NLMS algorithm [13] is applied. After channel estimation and data decision for the g th slot, the $2K$ -tap weight vector is updated. Updating of the tap weight vector $\{\mathbf{W}_{m,l,q}(g); q = 0 \sim Q-1\}$ without using the conjugate centrosymmetry property is expressed as

$$\begin{cases} \mathbf{W}_{m,l,q}(g+1) = \mathbf{W}_{m,l,q}(g) + \mu \frac{e_{m,l,q}(g)\mathbf{X}_{m,l}^*(g)}{\|\mathbf{X}_{m,l}(g)\|^2} \\ e_{m,l,q}(g) = \bar{\xi}_{m,l,q}(g) - \tilde{\xi}_{m,l}(g, n) \end{cases} \quad (10)$$

where $q = \lfloor \frac{n-N_p}{N_d/Q} \rfloor$ for $n = N_p \sim N_p + N_d - 1$,

$$\|\mathbf{X}_{m,l}(g)\|^2 = \sum_{k=-K+1}^K |\hat{\xi}_{m,l}(g+k)|^2 \quad (11)$$

is the Euclidean norm, $\{e_{m,l,q}(g); q = 0 \sim Q-1\}$ is the estimation error, and μ is the step size. $\bar{\xi}_{m,l,q}(g)$ is the reference signal for NLMS algorithm and is obtained by using decision feedback, reverse modulation and N_d/Q -symbol averaging as

$$\bar{\xi}_{m,l,q}(g) = \frac{Q}{N_d} \sum_{k=0}^{N_d/Q-1} \tilde{\xi}_{m,l}(g, N_p + qN_d/Q + k) \quad (12)$$

with

$$\tilde{\xi}_{m,l}(g, n) = r_{m,l}(g, n)\hat{d}^*(g, n), \quad (13)$$

where $\hat{d}(g, n)$ is the decision result on the n th symbol in the g th slot.

When the conjugate centrosymmetry property is used, $\{\mathbf{W}_{m,l,q}(g); q = 0 \sim Q/2-1\}$ are used for the first half interval ($n = N_p \sim N_p + N_d/2 - 1$) in a slot and $\{\mathbf{U}\mathbf{W}_{m,l,q}^*(g); q = 0 \sim Q/2-1\}$, which is the order-reversed version of the complex conjugate of $\mathbf{W}_{m,l,q}(g)$, are used for the second interval ($n = N_p + N_d/2 \sim N_p + N_d - 1$) in a slot, as shown in Eqs. (8a) and (8b). Therefore, $\{\mathbf{W}_{m,l,q}(g); q = 0 \sim Q/2-1\}$ used for the first half interval is reused for the second half interval. Updating of the tap weight vector $\{\mathbf{W}_{m,l,q}(g); q = 0 \sim Q/2-1\}$ using the conjugate centrosymmetry property is expressed as

$$\begin{cases} \mathbf{W}_{m,l,q}(g+1) = \mathbf{W}_{m,l,q}(g) + \mu \frac{e_{m,l,q}(g)\mathbf{X}_{m,l}^*(g)}{\|\mathbf{X}_{m,l}(g)\|^2} \\ e_{m,l,q}(g) = \bar{\xi}_{m,l,q}(g) - \tilde{\xi}_{m,l}(g, n) \\ \bar{\xi}_{m,l,q}(g) = \frac{Q}{N_d} \sum_{k=0}^{N_d/Q-1} \tilde{\xi}_{m,l}(g, N_p + qN_d/Q + k) \end{cases} \quad (14a)$$

where $q = \lfloor \frac{n-N_p}{N_d/Q} \rfloor$ for $n = N_p \sim N_p + N_d/2 - 1$, and

$$\begin{cases} \mathbf{W}_{m,l,q}(g+1) = \mathbf{W}_{m,l,q}(g) + \mu \left(\mathbf{U} \frac{e_{m,l,q}(g)\mathbf{X}_{m,l}^*(g)}{\|\mathbf{X}_{m,l}(g)\|^2} \right)^* \\ e_{m,l,q}(g) = \bar{\xi}_{m,l,q}(g) - \tilde{\xi}_{m,l}(g, n) \\ \bar{\xi}_{m,l,q}(g) = \frac{Q}{N_d} \sum_{k=0}^{N_d/Q-1} \tilde{\xi}_{m,l}(g, N_p + N_d/2 + qN_d/Q + k) \end{cases} \quad (14b)$$

where, $q = Q-1 - \lfloor \frac{n-N_p}{N_d/Q} \rfloor$ for $n = N_p + N_d/2 \sim N_p + N_d - 1$. In Eqs. (14a) and (14b), $\{e_{m,l,q}(g); q = 0 \sim Q/2-1\}$ is the estimation error.

When the common tap weight sets $\{\mathbf{W}_{l,q}^{(\text{com})}(g); q = 0 \sim Q/2-1\}$ for all antennas in addition to using the conjugate centrosymmetry property are used, updating of $\{\mathbf{W}_{l,q}^{(\text{com})}(g); q = 0 \sim Q/2-1\}$ is the same as in Eqs. (14a) and (14b), but with $\{\mathbf{W}_{m,l,q}(g); m = 0 \sim M-1\}$ replaced by $\{\mathbf{W}_{l,q}^{(\text{com})}(g)\}$.

Using the conjugate centrosymmetry property, the number of possible updates of each set of $2K$ tap weights in a slot becomes 2. Furthermore, using the same tap weight sets for all receive antennas, it increases to $2M$. Hence, it is expected that $2M$ times faster convergence rate can be achieved.

3. Computer Simulation

The computer simulation conditions are summarized in Table 1. We assume a frequency-selective Rayleigh fading channel with an $L=2$ -path uniform power delay profile, i.e., $E[|\xi_{m,l}(t)|^2] = 1/L$. Data modulation and spreading modulation are quadrature phase shift keying (QPSK) and binary PSK (BPSK), respectively. Since channel estimation accuracy depends on N_p , choice of N_p is important. As N_p increases, the SNR of the instantaneous channel estimate $\hat{\xi}_{m,l}(g)$ obtained by Eq. (4) improves due to coherent addi-

Table 1 Simulation condition.

Transmitter	Spreading factor	$SF=64$	
	Spreading sequence	Long PN sequence	
	Modulation	Data	QPSK
		Spreading	BPSK
Slot structure	Pilot	$N_p=4$ symbols	
	Data	$N_d=60$ symbols	
Propagation channel model	Rayleigh fading with $L=2$ -path uniform power delay profile		
Receiver	Diversity	$M=2$ -branch antenna diversity + L -finger rake	
	No. of tap weights	$2K=8$	

tion of N_p received pilot symbols. Accordingly, the BER performance improves. However, the transmission of too many non-information bearing pilot symbols degrades the BER performance due to the increase in power loss. From [10], we use $N_p=4$ and $N_d=60$ in the following computer simulations. For comparison, we also consider the pilot-assisted adaptive prediction channel estimation using linear interpolation [10] (hereafter, simply referred to as adaptive prediction channel estimation) and the WMSA channel estimation [6] using $K=1$ and 2 (the tap-weight vector is $\{0.5, 0.5\}$ for $K=1$ and $\{0.19, 0.31, 0.31, 0.19\}$ for $K=2$).

3.1 Convergence of Tap Weights

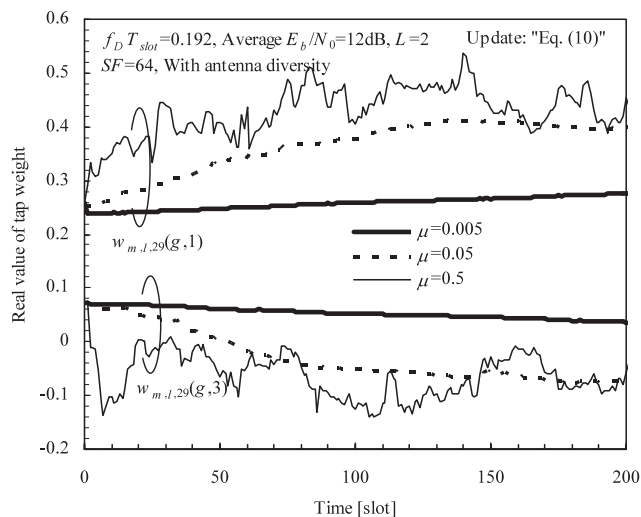
First, we evaluate the convergence rate of tap weights to select the step size in NLMS when the updating of Eq. (10a) is used. The normalized maximum Doppler frequency $f_D T_{slot}=0.192$ and no frequency offset $\Delta f=0$ are assumed. $Q = N_d (=60)$ sets of the $2K$ tap weights are used (i.e., each symbol position in a slot is provided a different set of $2K$ weights). Initial tap weight vector was set as $\mathbf{W}_{m,l,q}(0) = [0 + j0, 0.071 + j0, 0.19 + j0, 0.238 + j0, 0.238 + j0, 0.19 + j0, 0.071 + j0, 0 + j0]^T$ which corresponds to the tap weight vector of the $K=3$ -WMSA channel estimation [6].

Figure 4(a) shows the convergence performance of real part of $w_{m,l,29}(g, 1)$ and $w_{m,l,29}(g, 3)$ with μ as a parameter at the average received signal energy per bit-to-AWGN power spectrum density ratio E_b/N_0 per antenna=12 dB. As the step size μ becomes larger, the tap weight convergence rate becomes faster, but when $\mu=0.5$, tap weights are unstable. Therefore, $\mu=0.05$ is used in the following simulations.

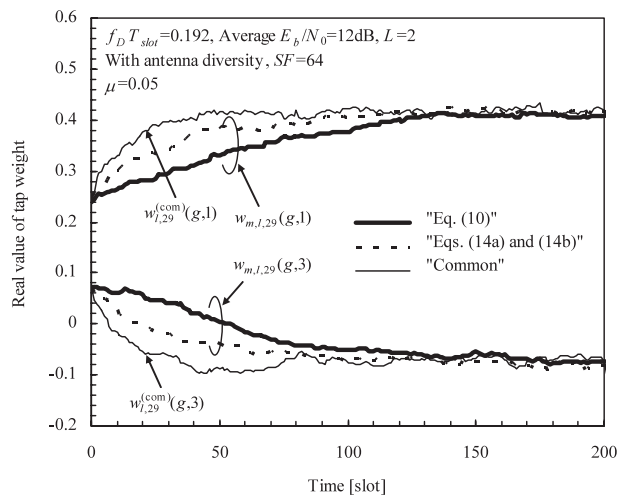
Figure 4(b) compares the convergence performances of three different tap adaptation methods described in Sect. 2.4. In the figure, "Eq. (10)" represents tap weight adaptation using Eq. (10) and "Eqs. (14a) and (14b)" represents the tap weight adaptation of Eqs. (14a) and (14b) using the conjugate centrosymmetry property. "Common" represents the tap weight adaptation sharing the common sets of tap weights for $M=2$ receive antennas in addition to using the conjugate centrosymmetry property. It is found from Fig. 4(b) that "Eqs. (14a) and (14b)" provides almost two times faster convergence rate than "Eq. (10)"; the tap weights converge after around 80 slots for "Eqs. (14a) and (14b)" while 150 slots for "Eq. (10)." Thus, the tap weight adaptation using the conjugate centrosymmetry property is useful. Furthermore, we can see that "Common" achieves much faster convergence than "Eqs. (14a) and (14b)."

3.2 BER Performance

The BER performance achievable with the proposed channel estimation scheme is compared with the WMSA channel estimation and the adaptive prediction channel estimation. First, we consider the case of no frequency offset Δf between a transmitter and a receiver. Figure 5 plots the average BER performances as a function of the average received E_b/N_0 per antenna for $L=2$ and $f_D T_{slot}=0.064$.



(a) Selection of step size.



(b) Comparison of three tap adaptation methods.

Fig. 4 Convergence performance.

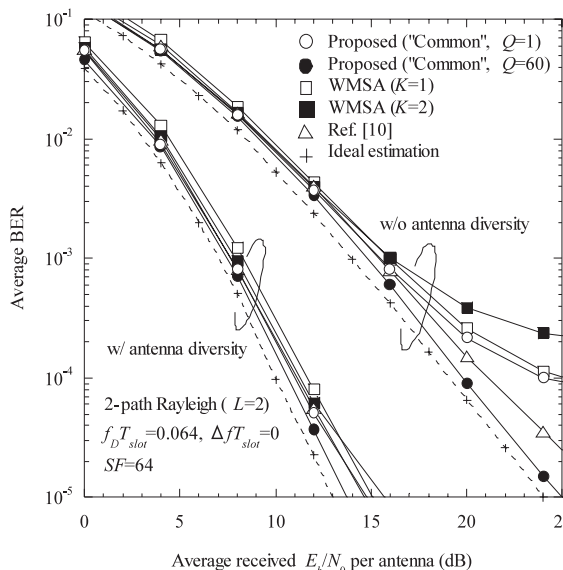


Fig. 5 BER performance comparison.

The WMSA channel estimation is designed to emphasize on reducing the noise effect at the cost of slightly losing the tracking ability against fading. In a low (high) E_b/N_0 region, $K=2(1)$ -WMSA channel estimation provides better BER performance than $K=1(2)$ -WMSA channel estimation. In a high E_b/N_0 region, the WMSA channel estimations do not perform well and produces the BER floors. However, the proposed adaptive channel estimation with $Q=60$ always provides the best BER performance. This is because the tap weight sets can be adapted to the changes in the average received E_b/N_0 and the better interpolation can be achieved using the $Q=60$ tap weight sets. The proposed channel estimation with $Q=60$ and 2-antenna diversity reception reduces the required average E_b/N_0 per antenna for $\text{BER}=10^{-4}$ by 0.6(0.4)dB compared with $K=1(2)$ -WMSA channel estimation and by 0.3dB compared with adaptive prediction channel estimation. The BER performance using the proposed adaptive channel estimation approaches that using ideal channel estimation and the degradation in E_b/N_0 for achieving $\text{BER}=10^{-4}$ is as small as 0.7 dB (0.28 dB out of which is due to the pilot insertion loss).

3.3 Impact of Fading Rate

Figure 6 shows how the fading rate impacts the channel estimation accuracy. The fading rate is represented by the normalized maximum Doppler frequency $f_D T_{slot}$. The average BERs at average received $E_b/N_0=12$ dB are plotted in the figure. It is seen that the proposed scheme with $Q=1$ provides almost the same BER as the $K=1$ -WMSA channel estimation, which uses one tap weight set of $\{0.5, 0.5\}$, because the tracking capability of both schemes against the fading is considered to be the same. This suggests that for obtaining the better BER performance, more than $Q=1$ tap weight sets should be used at the cost of increasing computational complexity (the effect of number of tap weight

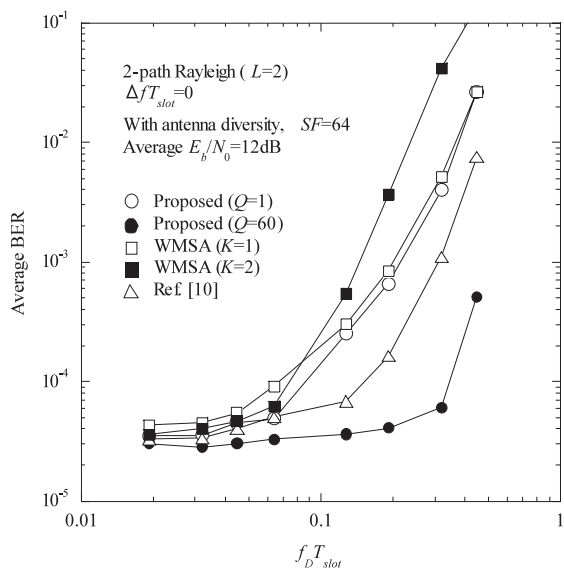


Fig. 6 Impact of normalized maximum Doppler frequency $f_D T_{slot}$.

sets will be discussed in Sect. 3.5). The proposed channel estimation scheme $Q=60$ achieves almost the same BER for $f_D T_{slot} < 0.2$. However, the BER achievable by the other channel estimation schemes rapidly increases as the value of $f_D T_{slot}$ increases, since the tracking ability of channel estimation against fading tends to be lost.

3.4 Impact of Frequency Offset

If the frequency offset is present between a transmitter and a receiver, the received signal experiences the constant phase rotation in addition to the random phase rotation due to fading. Figure 7 plots the average BER at average received $E_b/N_0=12$ dB as a function of the normalized frequency offset $\Delta f T_{slot}$. For very small values of $\Delta f T_{slot}$, the predominant cause of decision errors is the AWGN and hence, the BER is almost constant. As $\Delta f T_{slot}$ becomes larger, the BER starts to increase. However, the proposed adaptive channel estimation is very robust against the frequency offset, as well as fading as seen in Fig. 6.

3.5 Effect of Number of Tap Weight Sets

Reducing the number of tap weight sets reduces the receiver complexity; however, the achievable BER performance may degrade. This is because the same weight set is used for channel estimation at N_d/Q different symbol positions, although different symbol positions may experience different channel gains when fading is fast. Hence, the receiver complexity and the BER performance have a trade-off relation. Figure 8 plots the average BER performance as a function of Q for various values of $f_D T_{slot}$. As was expected, the BER increases as Q becomes smaller. However, sets of weights as small as $Q=6$ can be used (i.e., the number of tap weight sets can be reduced by 10 times) without sacrificing the BER performance when $f_D T_{slot} < 0.32$.

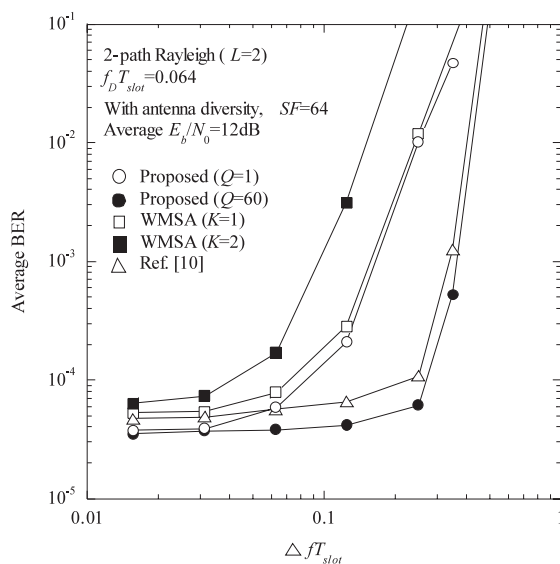


Fig. 7 Impact of normalized frequency offset $\Delta f T_{slot}$.

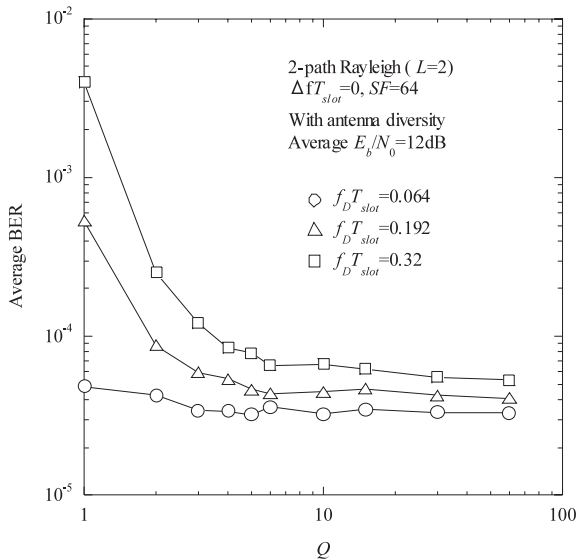


Fig. 8 Impact of number Q of available weight sets.

Table 2 Comparison of computational complexity.

Without conjugate centrosymmetry property		With conjugate centrosymmetry property	
N_d sets of tap weights (Eq. (5))	Q sets of tap weights (Eq. (5))	$Q/2$ sets of tap weights (Eqs. (8a) and (8b))	$Q/2$ sets of common tap weights for all receive antennas (Eqs. (9a) and (9b))
$2K \times N_d \times L \times M$	$2K \times Q \times L \times M$	$2K \times Q \times L \times M$	$2K \times Q \times L \times M$

3.6 Computational Complexity

The number of complex multiplication operations per slot is summarized in Table 2 for the proposed channel estimation schemes. The number of multiplication operations decreases Q/N_d times compared to using N_d tap weight sets, but, the additional reduction cannot be obtained by using the conjugate centrosymmetry property and by using the common tap weight sets for all receive antennas. However, the use of the conjugate centrosymmetry property and common tap weight sets can improve the convergence performance as shown in Fig. 4(b).

4. Conclusion

In this paper, a pilot-assisted channel estimation using adaptive interpolation was proposed to estimate the channel gains at different symbol positions for the coherent rake reception of DS-CDMA signals. Each set of interpolation filter tap weights is updated using the normalized least mean square (NLMS) algorithm. In order to reduce the number of tap weight sets and to achieve faster convergence of tap weights,

the conjugate centrosymmetry property is applied. The convergence rate and the average BER performance were evaluated by computer simulation in a frequency-selective Rayleigh fading channel. It was found that the tap adaptation method using the conjugate centrosymmetry property can achieve almost two times faster convergence rate. It was confirmed by computer simulation that the proposed adaptive channel estimation always provides a better BER performance than the conventional schemes and has very good robustness against fast fading and frequency offset. An E_b/N_0 degradation of as small as 0.7 dB from ideal channel estimation can be achieved at $BER=10^{-4}$ for two-path fading and $f_D T_{slot}=0.064$. Also, it was found that the number of tap weight sets can be reduced by 10 times (i.e., $Q=6$ without sacrificing the BER) when $f_D T_{slot} < 0.32$.

Acknowledgment

This work is supported by Grant-in-Aid for the Japan Society for the Promotion of Young Scientist.

References

- [1] F. Adachi, M. Sawahashi, and H. Suda, "Wideband DS-CDMA for next generation mobile communication system," IEEE Commun. Mag., vol.36, no.9, pp.56-69, Sept. 1998.
- [2] W.C. Jakes, Jr., ed., Microwave Mobile Communications, Wiley, New York, 1974.
- [3] J.K. Cavers, "An analysis of pilot symbol assisted modulation for Rayleigh fading channels," IEEE Trans. Veh. Technol., vol.40, no.4, pp.686-693, Nov. 1991.
- [4] S. Sampei and T. Sunaga, "Rayleigh fading compensation for QAM in land mobile radio communications," IEEE Trans. Veh. Technol., vol.42, no.2, pp.137-147, May 1993.
- [5] F. Ling, "Coherent detection with reference-symbol based estimation for direct sequence CDMA uplink communications," Proc. IEEE Vehicular Tech. Conference, pp.400-403, Secaucus, NJ, May 1993.
- [6] H. Andoh, M. Sawahashi, and F. Adachi, "Channel estimation filter using time-multiplexed pilot channel for coherent rake combining in DS-CDMA mobile radio," IEICE Trans. Commun., vol.E81-B, no.7, pp.1517-1526, July 1998.
- [7] S. Abeta, M. Sawahashi, and F. Adachi, "Performance comparison between time-multiplexed pilot channel and parallel pilot channel for coherent rake combining in DS-CDMA mobile radio," IEICE Trans. Commun., vol.E81-B, no.7, pp.1417-1425, July 1998.
- [8] M. Sakamoto, J. Huoponen, and I. Niva, "Adaptive channel estimation with velocity estimator for W-CDMA receiver," Proc. IEEE VTC2000-Spring, pp.2024-2028, Tokyo, May 2000.
- [9] S. Abeta, M. Sawahashi, and F. Adachi, "Adaptive channel estimation for coherent DS-CDMA mobile radio using time-multiplexing pilot and parallel pilot structures," IEICE Trans. Commun., vol.E82-B, no.9, pp.1505-1513, Sept. 1999.
- [10] S. Takaoka and F. Adachi, "Pilot-aided adaptive prediction channel estimation in a frequency-nonselective fading channel," IEICE Trans. Commun., vol.E85-B, no.8, pp.1552-1560, Aug. 2002.
- [11] M.D. Zoltowski, M. Haardt, and C.P. Mathews, "Closed form 2-D angle estimation with rectangular arrays in element space or beamspace via unitary ESPRIT," IEEE Trans. Signal Process., vol.44, no.2, pp.316-328, Feb. 1996.
- [12] N. Kikuma, Adaptive signal processing with array antenna, Science and Technology Publishing, 1999.
- [13] S. Haykin, Adaptive filter theory, 3rd ed., Prentice Hall, 1996.

- [14] Y. Honda and K. Jamal, "Channel estimation based on time-multiplexed pilot symbols," IEICE Technical Report, RCS96-70, Aug. 1996.

Appendix: Obtaining Eq. (7)

The optimum tap weight vector \mathbf{W}_q is given by [3], [13] (in the following, the antenna index m and path index l are omitted for simplicity)

$$\mathbf{W}_q = \left(\mathbf{R} + \frac{1}{SNR} \mathbf{I} \right)^{-1} \mathbf{r}_q, \quad (\text{A} \cdot 1)$$

where \mathbf{I} is an identity matrix and SNR denotes the average received signal-to-noise power ratio, \mathbf{R} is a $2K$ -by- $2K$ auto-correlation matrix whose element at the i th row and j th column is $\rho_{i,j}$, and $\mathbf{r}_q = [\kappa_{-K+1}^q, \kappa_{-K+2}^q, \dots, \kappa_K^q]^T$ is a $2K$ -by-1 cross-correlation vector whose i th element is κ_i^q . $\rho_{i,j}$ and κ_i^q are given by

$$\begin{cases} \rho_{i,j} = \text{E}[\xi^*(t + iT_{slot})\xi(t + jT_{slot})] \\ \quad \times \exp(j2\pi\Delta f(j - i)T_{slot}), \\ \quad \text{for } i, j = -K + 1 \sim K \\ \kappa_i^q = \text{E}[\xi^*(t)\xi(t + \Delta t)] \exp(j2\pi\Delta f\Delta t), \\ \quad \text{for } i = -K + 1 \sim K \end{cases} \quad (\text{A} \cdot 2)$$

where $\Delta t = iT_{slot} - \{N_p/2 + (2q + 1)N_d/(2Q)\}T$. Using $\text{E}[\xi(t)\xi^*(t + \Delta t)] = \text{E}[\xi^*(t)\xi(t - \Delta t)]$, we can show that

$$\kappa_i^q = \kappa_{-i+1}^{(Q-1)-q} \quad (\text{A} \cdot 3)$$

for $i = -K + 1 \sim K$ and hence

$$\mathbf{r}_q^* = \mathbf{U} \mathbf{r}_{(Q-1)-q}, \quad (\text{A} \cdot 4)$$

where \mathbf{U} is the $2K$ -by- $2K$ matrix given by

$$\mathbf{U} = \begin{pmatrix} 0 & \cdots & 0 & 1 \\ 0 & \cdots & 1 & 0 \\ \vdots & \ddots & \vdots & \vdots \\ 1 & \cdots & 0 & 0 \end{pmatrix}. \quad (\text{A} \cdot 5)$$

The matrix of \mathbf{U} reverses the element-order of a $2K$ -by-1 vector. Using Eqs. (A.1) and (A.4), we have

$$\begin{aligned} \mathbf{W}_q^* &= \left\{ \left(\mathbf{R} + \frac{1}{SNR} \mathbf{I} \right)^{-1} \right\}^* \mathbf{r}_q^* \\ &= \left\{ \left(\mathbf{R} + \frac{1}{SNR} \mathbf{I} \right)^{-1} \right\}^* \mathbf{U} \mathbf{r}_{(Q-1)-q}. \end{aligned} \quad (\text{A} \cdot 6)$$

Since $(\mathbf{R} + \mathbf{I}/SNR)$ is the Hermitian matrix, its inverse matrix is given by

$$\begin{aligned} \left(\mathbf{R} + \frac{1}{SNR} \mathbf{I} \right)^{-1} &= \left\{ \left(\mathbf{R} + \frac{1}{SNR} \mathbf{I} \right)^H \right\}^{-1} \\ &= \left\{ \left(\mathbf{R} + \frac{1}{SNR} \mathbf{I} \right)^{-1} \right\}^H, \end{aligned} \quad (\text{A} \cdot 7)$$

where $(\cdot)^H$ denotes the conjugate transpose operation. From Eq. (A.7), the inverse matrix of $(\mathbf{R} + \mathbf{I}/SNR)$ is also Hermitian matrix. Thus, $(\mathbf{R} + \mathbf{I}/SNR)^{-1}$ can be expressed as

$$\left(\mathbf{R} + \frac{1}{SNR} \mathbf{I} \right)^{-1} = \begin{pmatrix} v_0 & v_1 & \cdots & v_{2K-1} \\ v_1^* & v_0 & \cdots & v_{2K-2} \\ \vdots & \vdots & \ddots & \vdots \\ v_{2K-1}^* & v_{2K-2}^* & \cdots & v_0 \end{pmatrix}, \quad (\text{A} \cdot 8)$$

where the diagonal elements v_0 's are real and the other elements v_i 's ($i \neq 0$) are complex. Using Eqs. (A.5) and (A.8), we have

$$\begin{aligned} &\left\{ \left(\mathbf{R} + \frac{1}{SNR} \mathbf{I} \right)^{-1} \right\}^* \mathbf{U} \\ &= \begin{pmatrix} v_{2K-1}^* & v_{2K-2}^* & \cdots & v_1^* & v_0 \\ v_{2K-2}^* & v_{2K-3}^* & \cdots & v_0 & v_1 \\ \vdots & \vdots & \ddots & \vdots & \vdots \\ v_0 & v_1 & \cdots & v_{2K-2} & v_{2K-1} \end{pmatrix} \\ &= \begin{pmatrix} 0 & \cdots & 0 & 1 \\ 0 & \cdots & 1 & 0 \\ \vdots & \ddots & \vdots & \vdots \\ 1 & \cdots & 0 & 0 \end{pmatrix} \begin{pmatrix} v_0 & v_1 & \cdots & v_{2K-1} \\ v_1^* & v_0 & \cdots & v_{2K-2} \\ \vdots & \vdots & \ddots & \vdots \\ v_{2K-1}^* & v_{2K-2}^* & \cdots & v_0 \end{pmatrix} \\ &= \mathbf{U} \left(\mathbf{R} + \frac{1}{SNR} \mathbf{I} \right)^{-1}. \end{aligned} \quad (\text{A} \cdot 9)$$

Substituting Eq. (A.9) into Eq. (A.6), we obtain

$$\begin{aligned} \mathbf{W}_q^* &= \mathbf{U} \left(\mathbf{R} + \frac{1}{SNR} \mathbf{I} \right)^{-1} \mathbf{r}_{(Q-1)-q} \\ &= \mathbf{U} \mathbf{W}_{(Q-1)-q} \end{aligned} \quad (\text{A} \cdot 10)$$

and

$$\mathbf{W}_{(Q-1)-q} = \mathbf{U} \mathbf{W}_q^*. \quad (\text{A} \cdot 11)$$

It can be understood from Eq. (A.11) that \mathbf{W}_q and $\mathbf{W}_{(Q-1)-q}$ have the following conjugate centrosymmetry property [11], [12]:

$$\begin{aligned} w_{(Q-1)-q}(i) &= w_q^*(-i + 1) \quad \text{for } i = -K + 1 \sim K \\ \text{and } q &= 0 \sim Q - 1. \end{aligned} \quad (\text{A} \cdot 12)$$



Shinsuke Takaoka received his B.S. and M.S. degrees in communications engineering from Tohoku University, Sendai, Japan, in 2001 and 2003, respectively. Currently, he is a graduate student at the Department of Electrical and Communications Engineering, Tohoku University. His research interests include digital signal transmission techniques, especially for mobile communication systems.



Fumiya Adachi received his B.S. and Dr. Eng. degrees in electrical engineering from Tohoku University, Sendai, Japan, in 1973 and 1984, respectively. In April 1973, he joined the Electrical Communications Laboratories of Nippon Telegraph & Telephone Corporation (now NTT) and conducted various types of research related to digital cellular mobile communications. From July 1992 to December 1999, he was with NTT Mobile Communications Network, Inc. (now NTT DoCoMo, Inc.), where he

led a research group on wideband/broadband CDMA wireless access for IMT-2000 and beyond. Since January 2000, he has been with Tohoku University, Sendai, Japan, where he is a Professor of Electrical and Communication Engineering at Graduate School of Engineering. His research interests are in CDMA and TDMA wireless access techniques, CDMA spreading code design, Rake receiver, transmit/receive antenna diversity, adaptive antenna array, bandwidth-efficient digital modulation, and channel coding, with particular application to broadband wireless communication systems. From October 1984 to September 1985, he was a United Kingdom SERC Visiting Research Fellow in the Department of Electrical Engineering and Electronics at Liverpool University. He was a co-recipient of the IEICE Transactions best paper of the year award 1996 and again 1998. He is an IEEE Fellow and was a co-recipient of the IEEE Vehicular Technology Transactions best paper of the year award 1980 and again 1990 and also a recipient of Avant Garde award 2000.